Draft version July 26, 2021
Preprint typeset using LaTeX style emulateapj v. 6/22/04

A *SPITZER* STUDY OF DUSTY DISKS IN THE SCORPIUS-CENTAURUS OB ASSOCIATION

C. H. Chen[1], M. Jura[2], K. D. Gordon[3], M. Blaylock[3]

Draft version July 26, 2021

ABSTRACT

We have obtained *Spitzer Space Telescope* MIPS observations of 40 F- and G-type common proper motion members of the Scorpius-Centaurus OB Association with ages between 5 and 20 Myr at 24 μm and 70 μm. We report the detection of fourteen objects which possess 24 μm fluxes $\geq$30% larger than their predicted photospheres, tentatively corresponding to a disk fraction of $\geq$35%, including seven objects which also possess 70 μm excesses $\geq$100$\times$ larger than their predicted photospheres. The 24 μm plus 70 μm excess sources possess high fractional infrared luminosities, $L_{IR}/L_* = 7 \times 10^{-4}$ - 3 $\times$ 10^{-3}; either they possess optically thin, dusty β Pictoris-like disks or compact, opaque HD 98800-like disks.

Subject headings: stars: circumstellar matter— planetary systems: formation

1. INTRODUCTION

Circumstellar disks around young stars with ages <100 Myr are the likely birth places of planets and smaller bodies, analogous to asteroids, comets, and Kuiper-belt objects in our Solar System. However, how optically thick disks with interstellar gas-to-dust ratios evolve into Solar Systems is not well understood. Recent studies of the 10 Myr old TW Hydrae Association (Weinberger et al. 2004) and the 30 Myr Tucana-Horologium Association (Mamajek et al. 2004) find that warm circumstellar dust (T_{gr} = 200 - 300 K), if present, reradiates less than 0.1% - 0.7% of the stellar luminosity, $L_{IR}/L_* < 1$ - 7 $\times$ 10^{-3}. If the majority of stars possess Solar Systems, why do some stars, such as TW Hydrae, Hen 3-600, HD 98800 and HR 4796A in the TW Hydrae Association, still possess large quantities of gas and/or dust? In addition, the age $\sim$10 Myr appears to mark a transition in the gross properties of observed disks. Both optically thick, gaseous disks and optically thin, dusty disks have been discovered around 10 Myr old stars. Pre-main sequence T-Tauri and Herbig Ae/Be stars with ages <5 Myr typically possess both gas and dust while debris disks with ages >100 Myr are typically dusty and gas poor.

Detailed studies of the gas and dust content of 10 Myr old circumstellar disks suffer from small number statistics. Circumstellar disks around main sequence stars were discovered using the *IRAS* satellite (Backman & Paresce 1993); however, the sensitivity of *IRAS* limited studies of circumstellar disks to dust around T-Tauri stars, Herbig Ae/Be stars, and early-type main sequence stars. The excellent sensitivity of the *Spitzer Space Telescope* allows us not only to characterize better already known systems but also to identify previously unknown circumstellar disk systems around more distant objects and around fainter, later-type stars. We have obtained *Spitzer Space Telescope* MIPS observations of F- and G-type common proper motion members of the Scorpius-Centaurus OB Association with ages between 5 and 20 Myr to search for dusty circumstellar disks which may be transitioning from optically thick, gaseous systems to optically thin, dusty systems in order to understand better the evolution of gas and dust around young stars.

The Scorpius-Centaurus OB association, with typical stellar distances of 118 - 145 pc, is the closest OB assoication to the Sun and contains three subgroups: Upper Scorpius, Upper Centaurus Lupus, and Lower Centaurus Crux, with estimated ages of $\sim$5 Myr (Preibisch et al. 2002), 17 Myr, and 16 Myr (Mamajek, Meyer, & Liebert 2002) respectively. Member stars with spectral type F and earlier have been identified via common proper motion studies using *Hipparcos* data (de Zeeuw et al. 1999) while later-type members have been identified via indicators of youth (i.e. high coronal x-ray activity and large lithium abundance: Preibisch et al. 2002; Mamajek et al. 2002). The close proximity of Scorpius-Centaurus and the youth of its consituent stars make this association an excellent laboratory for studying the formation and evolution of planetary systems. A recent survey of 5 members of Upper Scorpius detected N-band excesses associated with two stars: J161411.0-230536 and HD 143006 (Mamajek et al. 2004).

We report a first set of results from a *Spitzer* search for dusty disks around 130 F-, G-, and K-type members of nearby (within 150 pc of the Sun) OB Associations using MIPS at 24 μm and 70 μm. We have obtained 24 μm and 70 μm photometry for 41 F- and G-type stars, including 5 members of Upper Scorpius, 11 members of Upper Centaurus Crux, and 25 members of Lower Centaurus Crux, whose membership has been determined via *Hipparcos* proper motion studies (de Zeeuw et al. 1999). Using Monte Carlo simulations, De Zeeuw et al. (1999) estimate that 32% of their proposed Lower Centaurus Crux members and 24% of their proposed Upper Centaurus Lupus members may be interlopers and not true association members because the stellar radial velocities are not measured. We cross-correlated our target list with published lists of confirmed and rejected Scorpius-Centaurus group members (Mamjek et al. 2002). One star (HD 113376) is excluded as a member based upon the lack of youth indicators (Hα emission, *ROSAT* flux, lithium abundance). Four others (HD 105070, HD 108568, HD

[1] National Research Council Resident Research Associate, Jet Propulsion Laboratory, M/S 169-506, California Institute of Technology, 4800 Oak Grove Drive, Pasadena, CA 91109; christine.chen@jpl.nasa.gov
[2] Department of Physics and Astronomy, University of California, Los Angeles, CA 90095-1562; jura@astro.ucla.edu
[3] Steward Observatory, University of Arizona, Tucson, AZ 85721

108611, HD 119022, HD 138009) are confirmed as members from their subgiant surface gravities, high lithium abundances, strong x-ray emission (L_x = 10^{29} - 10^{30} ergs s^{-1}), and proper motions consistent with the high mass members. We list the targets along with their spectral types, distances, V-band extinctions (Sartori et al. 2003), *ROSAT* fluxes, and OB Association subgroup memberships in Table 1.

2. OBSERVATIONS

Our data were obtained using the Multiband Imaging Spectrometer for *Spitzer* (MIPS) (Rieke et al. 2004) on the *Spitzer Space Telescope* (Werner et al. 2004) in photometry mode at 24 μm and 70 μm (default scale). Each of our targets was observed either during 20 - 26 February 2004 or during 14 - 22 March 2004 using integration times of 48.2 sec at 24 μm and 93 sec at 70 μm. The data were reduced and combined using the Data Analysis Tool (DAT) version 2.80 developed by the MIPS instrument team (Gordon et al. 2004). Extra processing steps beyond those in the DAT were applied to remove known transient effects associated with the 70 micron detectors to achieve the best possible sensitivity. While point sources are well calibrated using the stim flashes, extended sources (eg., the background) show small responsivity drifts with respect to the point source calibration. As a result, the background in uncorrected mosaics displays significant structure associated with detector columns. This detector dependent structure is removed by subtracting column averages from each exposure with the source region masked. In addition, a pixel dependent time filter is applied (with the source region masked) to remove small pixel dependent residuals. These corrected images are then combined to produce the final mosaic used for the source detection.

The estimated 70 μm sky backgrounds, extrapolated from COBE data, using the IRSKY Batch Inquiry System (IBIS), suggest that our fields-of-view possess medium to high 70 μm cirrus backgrounds (see Table 2). To avoid confusion with cirrus clumps, we visually searched for bright sources in each of our 70 μm fields-of-view. If no object was detected at the center of the array, we placed detection limits on the fluxes, computed from the sky noise measured in a background annulus. This sky noise includes detector noise and noise due to cirrus structures present in the image. Since these observations were taken in a region with high cirrus, the detection limits are dominated by cirrus noise. In fact, examination of the 70 micron images reveals significant cirrus structures which make our simple aperture photometry detection limits conservative upper limits.

We used aperture photometry to measure the fluxes, by finding the average brightness of a pixel in a "sky" annulus around the source, subtracting this value from each pixel in the aperture, and then summing the flux in the aperture. Since our observations are diffraction limited and the pixel scale for the 24 μm and 70 μm detectors are different, we use different aperture radii and sky annuli for the 24 μm and 70 μm data. We used 15″ (6 pixel) and a 29.5″ (3 pixel) radius apertures to estimate the source flux and 30″ (12 pixel) to 43″ (17 pixel) and 40″ (4 pixel) to 80″ (8 pixel) sky annuli to estimate the sky backgrounds at 24 μm and 70 μm, respectively. These apertures are not large enough to contain all of the photons from a diffraction limited point source; therefore, we applied scalar aperture corrections of 1.147 and 1.267 at 24 μm and 70μm, respectively, inferred from *Spitzer* Tiny Tim models of the Point Spread Function (Krist 2002), to extrapolate the object fluxes from the photon fluxes in the apertures. We flux calibrated our data assuming conversion factors of 1.042 μJy arcsec^{-2}/(DN sec^{-1}) at 24 μm and 1.58×10^4 μJy arcsec^{-2}/(DN sec^{-1}) at 70 μm. We list the uncolor-corrected observed 24 μm and 70 μm fluxes in Table 2. Current observations of standard stars suggest that MIPS 24 μm photometry has an uncertainty of ∼10% for stars fainter than 4 Jy and that MIPS 70 μm photometry has an uncertainty of ∼20% for objects brighter than 50 mJy.

We modeled the stellar photospheres of our objects by minimum χ^2 fitting extinction corrected published photometry from the literature, using fluxes at wavelengths shorter than 3 μm, to 1993 Kurucz stellar atmospheres using the package Best Kurucz developed by the MIPS instrument team (Su et al. 2004). We input measured extinctions, A_V, stellar effective temperatures, T_*, and gravities, $\log g$, from Sartori et al. (2003), extinction-corrected the fluxes using the Cardelli, Clayton, & Mathis (1989) extinction law, searched a grid of parameter space around our assumed values, and found an atmosphere model (effective temperature, metallicity, gravity) which fit the data the best. Where possible, we included fluxes from TD 1 (Thompson et al. 1978), *Hipparcos*, the General Catalog of Photometric Data (Mermilliod, Mermilliod, & Hauck 1997), and 2MASS (Cutri et al. 2003). For comparison with our uncolor-corrected, measured fluxes, we list the predicted 24 μm and 70 μm fluxes integrated over the MIPS bandpasses in Table 2.

3. EXCESS STATISTICS

Fourteen objects in our sample (>35%) possess 24 μm fluxes ≥30% larger than their predicted photospheres. Seven of which (HD 106906, HD 113556, HD 113766, HD 114082, HD 115600, HD 117214, HD 152404) are detected at 70 μm and possess 70 μm excesses ≥100× larger than their predicted photospheres. The 24 μm and 70 μm fluxes are probably not interstellar because the point source, at the *Hipparcos* positions of the stars, are detected with good contrast to the sky. With the exception of AK Sco (HD 152404), the 24 μm plus 70 μm excess sources are members of Lower Centaurus Crux with estimated ages ∼16 Myr. Seven of our 24 μm excess objects (HD 103234, HD 103703, HD 104231, HD 111102, HD 119511, HD 133075, HD 148040) are not detected at 70 μm. Five of these objects (HD 103234, HD 103703, HD 104231, HD 111102, HD 119511) are members of Lower Centaurus Crux, one is a member of Upper Centaurus Lupus (HD 133075), and one is a member of Upper Scorpius (HD 148040). We infer association subgroup disk fractions of 46%, 9%, and 20% for each of the Scorpius-Centaurus subgroups respectively from our 24 μm excess sources. Since our sample was selected on the basis of common proper motion, ∼30% of our sample may be interlopers, suggesting that the the Sco-Cen disk fractions measured in this study may be as much as 40% higher than quoted above. More accurate measurements of the disk fractions will be made once all of the scheduled *Spitzer* MIPS observations are completed. The existence of so many 24 μm excess sources may not be surprising.

A $JHKL$ search for near-infrared excesses in the 5-8 Myr η Cha cluster revealed hot inner disks around 60% (9 out of the 15) of the sources searched (Lyo et al. 2003).

For each 24 μm plus 70 μm excess source, we fit the MIPS 24 μm and 70 μm excess fluxes with a single temperature black body, T_{gr}, (see Figure 2), and infer color temperatures, T_{gr} = 65 - 330 K, and fractional infrared luminosities, $L_{IR}/L_* = 7 \times 10^{-4}$ - 3×10^{-3}. Fitting a simple black body to broad-band photometry often underestimates the dust grain temperature because the real grain emissivity falls more rapidly at wavelengths $\lambda > 2\pi a$. We additionally fit the 24 μm and 70 μm photometry assuming an emissivity Q_λ = constant for $\lambda < 2\pi a$ and Q_λ = constant $(2\pi a/\lambda)^{1.5}$ for $\lambda > 2\pi a$ (Backman & Paresce 1993). For HD 113766, this emissivity law is unable to reproduce simultaneously the IRAS 12 μm, the MIPS 24 μm, and the MIPS 70 μm fluxes. If the MIPS 24 μm and 70 μm fluxes are used to constrain the SED, this model predicts a 12 μm flux which is significantly higher than observed while the simple black body is able to reproduce both the MIPS and IRAS data sets. To be consistent, we have used a simple black body to model all of the objects in our sample. Recent *Spitzer* IRS spectra have revealed the lack of 10 μm and 20 μm silicate features around debris disks, suggesting that the grains in these systems have diameters larger than 10 μm (Jura et al. 2004). We can not constrain the color temperatures of the 24 μm excess only sources without infrared excess detections at another wavelength. We infer the fractional dust luminosities for 24 μm excess only sources assuming $F_{IR} \approx \nu F_\nu(24\ \mu\text{m})$. Our constraint on the 70 μm fluxes of the 24 μm excess-only sources suggests that the color temperatures for these sources is significantly warmer. These sources may be circumstellar disks with warmer dust grains or they may be entirely different objects altogether.

4. OPTICALLY THIN DISKS?

One possibility is that these dusty disks are optically thin. The high fractional infrared luminosities, L_{IR}/L_* = 7×10^{-4} - 3×10^{-3}, associated with stars with ages $\sim$16 Myr, suggests that these objects may be similar to β Pictoris which possesses $L_{IR}/L_* = 10^{-3}$ at an age of 12 Myr. The observed 24 μm and 70 μm infrared excesses can be modeled using an optically thin dust distribution as described below.

4.1. *Circumstellar Dust Grain Size*

A lower limit to the size of dust grains orbiting a star can be found by balancing the force due to radiation pressure with the force due to gravity. For small grains with radius a, the force due to radiation pressure overcomes gravity for:

$$a < 3L_* Q_{pr}/(16\pi G M_* c \rho_s) \quad (1)$$

(Artymowicz 1988) where Q_{pr} is the radiation pressure coupling coefficient and ρ_s is the density of an individual grain. Since radiation from F- and G-type stars is dominated by ultraviolet and visual light, we expect that $2\pi a/\lambda \gg 1$ and therefore the effective cross section of the grains can be approximated by their geometric cross section so $Q_{pr} \approx 1$. Based upon T_* and L_*, the inferred stellar masses are 1.4 - 1.8 $M_\odot$ (Siess, Dufour, & Forestini 2000). With ρ_s = 2.5 g cm^{-3}, the minimum radii for grains orbiting our 24 μm plus 70 μm excess objects are a = 0.5 - 1.9 μm.

We can estimate the average size of the grains assuming a size distribution for the dust grains. As expected from equilibrium between production and destruction of objects through collisions (Greenberg & Nolan 1989), we assume

$$n(a)da = n_o a^{-p} da \quad (2)$$

with p $\simeq$ 3.5 (Binzel, Hanner, & Steel 2000). If we assume a minimum grain radius of 0.5 - 1.9 μm, we find an average grain radius $< a > =$ 0.8 - 3.3 μm, if we weight by the number of particles.

4.2. *Mass of Circumstellar Dust*

The characteristic grain distance can be constrained from the temperature of the grains assuming that they are black bodies. We estimate grain temperatures of T_{gr} = 65 - 330 K from the ratio of the 24 μm excesses to 70 μm excesses. Black bodies in radiative equilibrium with a stellar source are located a distance

$$D = \frac{1}{2}\left(\frac{T_*}{T_{gr}}\right)^2 R_* \quad (3)$$

from the central star (Jura et al. 1998), where T_* and R_* are the effective temperature of the stellar photosphere and the stellar radius. We use stellar luminosities, L_*, from Sartori et al. (2003) and our inferred stellar effective temperatures, T_*, with stellar evolution models (Siess, Dufour, & Forestini 2000) to infer stellar radii, R_*, and masses, M_*, where possible. For objects with L_* and T_* which do not appear on model grids, we infer stellar radii from $L_* = 4\pi R_*^2 \sigma T_*^4$. From equation (1) and the stellar properties summarized in Table 3, we find characteristic grain distances of 2.9 AU - 40 AU.

We can estimate the minimum mass of dust assuming that the particles have $< a > \sim$ 0.8 - 3.3 μm; if the grains are larger, then our estimate is a lower bound. If we assume a thin shell of dust at distance, D, from the star and if the particles are spheres of radius, a, and if the cross section of the particles equals their geometric cross section, then the mass of dust is

$$M_d \geq \frac{16}{3}\pi \frac{L_{IR}}{L_*} \rho_s D^2 < a > \quad (4)$$

(Jura et al. 1995) where L_{IR} is the luminosity of the dust. From equation (3) and the stellar properties summarized in Table 3, we infer dust masses, M_{dust} = 7 $\times 10^{-4}$ - 2×10^{-2} M_{moon}.

4.3. *Stellar Wind Drag*

Stellar wind drag effectively removes small dust particles around young F- and G-type stars. We can compare the mass loss rate from stellar wind drag to that of the Poynting-Robertson effect, the dominant grain removal mechanism in debris disks around main sequence A-type stars and in our Solar System. The increase in "drag" in the inward drift velocity over that produced by the Poytning-Robertson effect is given approximately by the factor $(1 + \dot{M}_{wind} c^2/L_*)$, where $\dot{M}_{wind}$ is the stellar wind mass loss rate and L_* (Jura 2004). For our solar system, $\dot{M}_{wind} = 2 \times 10^{12}$ g/sec or $\dot{M}_{wind} c^2/L_\odot = 0.5$.

We infer $\dot{M}_{wind}$ from *ROSAT* fluxes for our sample using the observed dependence of stellar mass loss

rate, $\dot{M}_{wind}$, per stellar surface area, A, on x-ray flux per stellar area for nearby G-, K- and, M-type stars $\dot{M}_{wind}/A \propto F_x^{1.15\pm0.2}$ scaled to observations of 36 Oph ($F_x = 3.6 \times 10^5$ erg cm^{-2} s^{-1}, $\dot{M}_{wind}/A = 17\ \dot{M}_\odot/A_\odot$; Wood et al. 2002). Using the *ROSAT* fluxes listed in Table 1, we estimate $\dot{M}_{wind}c^2/L_\odot = 76$, 27, 15 and 77 for HD 103234, HD 104231, HD 113766, and HD 148040 respectively, suggesting that stellar wind drag is more important than the Poynting-Robertson effect for all of these systems. The nondetection of the remaining sources in the *ROSAT* All-Sky Bright Source and the *ROSAT* All-Sky Survey Faint Source Catalogs suggests that they possess 0.2 - 2.0 keV fluxes <0.05 counts/sec. For these objects, we can not place strong constraints on $\dot{M}_{wind}c^2/L_\odot$ to determine the relative importance of stellar wind drag and the Poynting-Robertson effect; however, the stellar wind mass loss rates are expected to be similar to the other stars in the sample. Solar evolutionary models allow for a Sun which, at an age of 20 Myr, possesses a mass loss rate as high as, $\dot{M}_{wind} = 2 \times 10^{15}$ g s^{-1} (Sackmann & Boothroyd 2003), suggesting $\dot{M}_{wind}c^2/L_\odot = 460$.

4.4. *Lifetime of Circumstellar Grains*

We can estimate the lifetime of circumstellar dust grains assuming that stellar wind drag is the dominant removal mechanism. The speed at which particles drift radially inward under the Poynting-Robertson effect and stellar wind drag is

$$v = \left(\frac{3L_*}{8\pi a \rho_s c^2 D}\right)\left(1 + \frac{\dot{M}_{wind}c^2}{L_*}\right) \quad (5)$$

(Burns, Lamy, & Soter 1979; Gustafson 1994); therefore, the lifetime for particles under stellar wind drag, t_{drag}, in environments in which stellar wind drag is much larger than the Poynting-Robertson effect ($\dot{M}_{wind}c^2/L_* >> 1$) is:

$$t_{drag} = \frac{4\pi < a > \rho_s D^2}{3\dot{M}_{wind}} \quad (6)$$

For HD 113766, if $< a > = 3.3$ μm, $\rho_s = 2.5$ g cm^{-3}, $D = 2.9$ AU, $\dot{M}_{wind} = 760\ \dot{M}_\odot$, then $t_{drag} = 12{,}000$ yr. Since this timescale is significantly shorter than the stellar age (t_{age}), we hypothesize that the grains are replenished by collisions between larger bodies. This system may be a younger, lower mass analog to ζ Lep, a 200 Myr A3V member of the Castor Moving Group, located 19 pc away from the Sun (Barrado y Navascués 1998) which possesses dust at terrestrial temperatures, $T_{gr} \sim 300$ K. Since the Poynting-Robertson drag lifetime of dust grain in this system is 10,000 years, the dust grains must be replenished by collisions between asteroidal bodies. High resolution 11.7 μm and 17.9 μm imaging and photometry confirmed that the dust grains are are located at a distance $\leq$6 AU from the star (Chen & Jura 2001).

4.5. *Minimum Mass of the Parent Bodies*

We can estimate the minimum mass in parent bodies assuming that the system is in a steady state and that the minimum mass is larger than the mass already removed by the stellar wind during the lifetime of the star. If M_{PB} denotes the minimum parent body mass, then we may write

$$M_{PB} \geq \dot{M}_{dust} t_{age} \quad (7)$$

where $\dot{M}_{dust}$ is the dust removal rate

$$\dot{M}_{dust} = \dot{M}_{wind}\frac{L_{IR}}{L_*} \quad (8)$$

Jura (2004). Using equation (8), stellar wind mass loss rates inferred from *ROSAT* fluxes given in Table 1 and fractional infrared luminosities listed in Table 3, we infer $\dot{M}_{dust} < 2 \times 10^{-6}\ M_{moon}$/yr for all of the 24 μm excess systems. Using equations (7) and (8), we estimate:

$$M_{PB} \geq \frac{L_{IR}}{L_*}\dot{M}_{wind} t_{age} \quad (9)$$

From equation (9) and the stellar properties listed in Tables (1) and (3), we infer parent body masses $M_{PB} = 0.3$ - 10 M_{moon}, approximately 10 times the mass of the Main Asteroid Belt in our Solar System. The largest minimum parent body mass, 10 M_{moon}, is close to 0.2 $M_\oplus$, suggesting that these systems may possess environments in which planets may be forming.

5. FLAT, OPTICALLY THICK DISKS?

The candidate disks, discovered in this survey, have approximately the same 70 μm luminosity. One natural explanation for the convergence of the 70 μm luminosities is that the disks are optically thick and geometrically thin, similar to the disk found around the 10 Myr old TW Hydrae Association object HD 98800. Face-on, opaque, geometrically thin disks with inner holes can be constructed so that they possess color temperatures consistent with the MIPS data.

The predicted temperature structure for a geometrically flat, passive, optically thick circumstellar disk is

$$T_{disk} = \left(\frac{2}{3\pi}\right)^{1/4}\left(\frac{R_*}{R}\right)^{3/4} T_* \quad (10)$$

(Jura 2003). The predicted flux density for the same disk with an inclination, i, at a frequency, ν, is

$$F_\nu = 12\pi^{1/3}\frac{R_*^2 \cos i}{D_*^2}\left(\frac{2k_B T_*}{3h\nu}\right)^{8/3}\frac{h\nu^3}{c^2}\int_{x_{in}}^{x_{out}}\frac{x^{5/3}}{e^x - 1}dx \quad (11)$$

(Jura 2003) where $x = h\nu/k_B T_{disk}$ and D_* is the distance to the star. We use the measured $F_\nu(24\ \mu\text{m})/F_\nu(70\ \mu\text{m})$ flux ratio to constrain the inner radii for the disks, assuming that they have $R_{out} = \infty$, and the magnitude of the 24 μm flux to infer the disk inclinations. For example, for HD 106906 with $D_* = 92$ pc, $T_* = 6750$ K, and $R_* = 1.6\ R_\odot$, we estimate an inner radius, $R_{in} = 0.68$ AU and an inclination, $i = 68$ °. The measured fluxes are approximately a factor of 2 smaller than the maximum value allowed for an opaque, flat disk. The fact that (1) the measured fluxes are so close to the maximum allowed value and (2) the estimated inclination angles appear to cluster around 65° may suggest saturation in our model. The saturation may be the result of our simple grain assumptions. We have not considered the possibility that circumstellar dust grains might reflect some of the incident stellar radiation as observed in some circumstellar disks. If the albedo in these systems is ~0.5, then the

predicted 24 μm and 70 μm fluxes would be reduced by a factor of 2. Spatially resolved scattered light imaging, combined with thermal mid-infrared imaging of the HD 141569, suggest that the albedo in this system is ∼0.4, similar to the values inferred for Herbig Ae/Be stars using *ISO* (Weinberger et al. 1999). Our inferred disk inner radii are similar to those inferred for T-Tauri disks. Near-infrared spectroscopy suggests that the inner radii of T-Tauri disks are located at the dust sublimation radii, R_{in} = 0.07-0.5 AU, further than expected if the dust is heated by the luminosity of the star alone because the disk is heated by both the stellar luminosity and accretion onto the star (Muzzerolle et al. 2003). Whether these systems are continuing to accrete gas is not obervationally known.

One star which does not fit the model of an optically thick, geometrically thin disk with an inner hole is HD 113766 which possess a significantly stronger 24 μm excess than a 70 μm excess. For HD 113766, we use the measured $F_\nu(2.2\ \mu\mathrm{m})/F_\nu(24\ \mu\mathrm{m})$ and the measured $F_\nu(24\ \mu\mathrm{m})/F_\nu(70\ \mu\mathrm{m})$ flux ratios to constrain the inner and outer radii for the disk; however, we were unable to scale the magnitude of the 24 μm flux to estimate the disk inclination. The dusty disk around HD 113766 produces more radiation than can be produced by an optically thick, geometrically thin disk.

6. DISCUSSION

The current data do not allow us to determine whether these dusty disks possess grains at a single radius or whether they possess continuous disks (for example, disks whose surface density distributions are determined by infall under stellar wind drag), or whether they possess flat, optically thick disks.

Although coronal x-ray emission is used as an indicator for youth among later-type stars, it may not be correlated with the presence of infrared excess indicative of the presence of circumstellar dust. In Figure 3, we show the observed x-ray luminosities (L_x/L_{bol}), inferred from *ROSAT* observations using the conversion 1 *ROSAT* count = (8.31 + 5.30×HR1) 10^{-12} erg cm^{-2} (Fleming et al. 1995), where HR1 is the hardness ratio between the 0.1 - 0.4 keV and the 0.5 - 2.0 keV bands, plotted as a function of infrared luminosity (L_{IR}/L_{bol}), inferred from MIPS 24 μm excesses using $L_{IR} = \nu L_\nu(24\ \mu\mathrm{m})$. Contrary to expectation, the infrared luminosity appears anticorrelated with x-ray luminosity expect for 30% of the objects which possess neither a *ROSAT* flux nor a MIPS 24 μm excess. The anticorrelation can be naturally explained if stellar wind drag effectively removes dust grains around young stars with high x-ray coronal activity. The objects that lack both a *ROSAT* flux and a MIPS 24 excess may be the ∼30% interlopers predicted by de Zeeuw et al. (1999). Recent *Chandra* observations of HD 98800, a quadruple system in the ∼10 Myr old TW Hydrae Association, have revealed that the x-ray flux of the dusty binary system HD 98800B is ∼4 times fainter than its dustless companion HD 98800A (Kastner et al. 2004). Since the x-ray luminosities of solar-like stars vary with time, more observations of HD 98800 are needed to determine whether the measured anticorrelation between infrared luminosity and x-ray luminosity is an effect of observing the system at a special time.

Recent ground-based searches for new 10 μm and 20 μm excesses around proper motion and x-ray selected K- and M-type members of the ∼10 Myr old TW Hydrae Association (Weinberger et al. 2004) and around proper motion, x-ray and lithium selected F-, G-, K-, and M-type members of the ∼30 Myr old Tucana-Horologium Association (Mamajek et al. 2004) have been relatively unsuccesful. The observed anti-correlation between x-ray luminosity and infrared luminosity may help explain the lack of infrared excess sources found in the TW Hydrae and Tucana-Horologium Assoications.

7. CONCLUSIONS

We have obtained MIPS 24 μm and 70 μm photometry of 40 F- and G-type stars in Scorpius-Centaurus using MIPS on the *Spitzer Space Telescope*.

1. Fourteen targets possess 24 μm excesses, corresponding to a 35% disk fraction in Scorpius-Centaurus. If the interlopers in the study do not possess infrared excess and are excluded, then the disk fraction may be as high as 50%. Half of the 24 μm excess sources also possess 70 μm fluxes >100× larger than expected from their photospheres alone.

2. The sources with 24 μm plus 70 μm excesses possess grain temperatures, T_{gr} = 65 - 310 K and high fractional infrared luminosities $L_{IR}/L_* = 7.0\ \times 10^{-4}$ - 0.019 suggesting that these systems may possess optically thin, β Pictoris-like dusty disks or compact, optically thick HD 98800-like disks.

3. The observed fractional infrared luminosities of dusty disks appear anticorrelated with *ROSAT* x-ray fluxes and may help explain the difficulty of finding dusty disks around stars which were identified to be young using x-ray observations.

We would like to thank V. Krause, J. Stansberry, and K. Su for their assistance with the MIPS DAT and/or the photosphere fitting tools. We would like to thank G. Bryden, E. Mamajek, and M. Werner for their comments and suggestions. This work is based on observations made with the *Spitzer Space Telescope*, which is operated by the Jet Propulsion Laboratory, California Institute of Technology under NASA contract 1407.

REFERENCES

Artymowicz, P. 1988, ApJ, 335, L79
Backman, D. E., & Paresce, F. 1993, in Protostars and Planets III, eds. E. Levy and J. I. Lunine (Tuscon: University of Arizona Press), 1253
Barrado y Navascués, D. 1998, A&A, 339, 831
Binzel, R. P., Hanner, M. S., & Steel, D. I. 2000, in Allen's Astrophysical Quantities, ed. A. N. Cox (New York: Springer-Verlag), 315
Burns, J. A., Lamy, P. L., & Soter, S. 1979, Icarus, 40, 1
Cardelli, J. A., Clayton, G. C., & Mathis, J. S. 1989, ApJ, 345, 245
Chen, C. H., & Jura, M. 2001, ApJ, 560, L171
Cutri, R. M., Skrutskie, M. F., van Dyk, S., Beichman, C. A., Carpenter, J. M., Chester, T., Cambresy, L., Evans, T., et al. 2003, 2MASS All-Sky Catalog of Point Sources (IPAC/California Institute of Technology)
de Zeeuw, P. T., Hoogerwerf, R., de Bruijne, J. H. J., Brown, A. G. A., & Blaauw, A. 1999, AJ, 117, 354
ESA, 1997, The Hipparcos and Tycho Catalogues (ESA SP-1200)

Fleming, T. A., Molendi, S., Maccacaro, T., & Wolter, A. ApJS, 99, 701
Gordon, K. 2004, PASP, submitted
Greenberg, R., & Nolan, M. C. 1989, in Asteroids II, eds. R. P. Binzel, T. Gehrels & M. S. Matthews (Tuscon: University of Arizona Press), 778
Gustafson, B. A. S. 1994, Annu. Rev. Earth Planet. Sci., 22, 553
Jura, M., Ghez, A. M., White, R. J., McCarthy, D. W., Smith, R. C., & Martin, P. G. 1995, ApJ, 445, 451
Jura, M., Malkan, M., White, R., Telesco, C., Pina, R., & Fisher, R. S., 1998, ApJ, 505, 897
Jura, M. 2003, ApJ, 584, L91
Jura, M. 2004, ApJ, 603, 729
Jura, M., Chen, C. H., Furlan, E., Green, J., Sargent, B., Forrest, W. J., Watson, D. M. et al. 2004b, ApJS, 154, 453
Kastner, J. H., Huenemoerder, D. P., Schulz, N. S., Canizares, C. R., Li, J., & Weintraub, D. A. 2004, ApJ, 605, L49
Krist, J. 2002, "Tiny Tim/SIRTF User's Guide, Spitzer Science Center internal document
Kenyon, S. J., & Hartmann, L. 1995, ApJS, 101, 117
Lyo, A.-R., Lawson, W. A., Mamajek, E. E., Feigelson, E. D., Sung, E.-C., Crause, L. A. 2003, MNRAS, 338, 616
Mamajek, E. E., Meyer, M. R., & Liebert, J. 2002, ApJ, 124, 1670
Mamajek, E. E., Meyer, M. R., Hinz, P. M., Hoffman, W. F., Cohen, M., & Hora, J. L. 2004, ApJ, 612, 496
Mermilliod, J.-C., Mermilliod, M., & Hauck, 1997, A&AS, 124, 349
Muzerolle, J., Calvet, N., Hartmann, L., & D'Alessio, P. 2003, ApJ, 597, L149
Preibisch, T., Brown, A. G. A., Bridges, T., Guenther, E., & Zinnecker, H. 2002, ApJ, 124, 404
Rieke, G., Young, E. T., Engelbracht, C. W., Kelly, D. M., Low, F. J., Haller, E. E.,Beeman, J. W., Gordon, K. D. et al. 2004, ApJS, 154, 25
Sackmann, I.-J., & Boothroyd, A. I. 2003, ApJ, 583, 1024
Sartori, M. J., Lepine, J. R. D., & Dias, W. S. 2003, A&A, 404, 913
Siess, L., Dufour, E., & Forestini, M. 2000, A&A, 358, 593
Su, K. 2004, in preparation
Thompson, G. I., Nandy, K., Jamar, C., Monfils, A., Houziaux, L., Carnochan, D. J., & Wilson, R. 1978, Catalog of Stellar Ultraviolet Fluxes (ESA SR-28)
Weinberger, A. J., Becklin, E. E., Zuckerman, B., & Song, I. 2004, 127, 2246
Weinberger, A. J., Becklin, E. E., Schneider, G., Smith, B. A., Lowrance, P. J., Silverstone, M. D., Zuckerman, B., & Terrile, R. J. 1999, ApJ, 525, L53
Werner, M., Roellig, T., Low, F., Rieke, G., Rieke, M., Hoffmann, W., Young, E., Houck, J. et al. 2004, ApJS, in press
Wood, B. E., Muller, H.-R., Zank, G. P., & Linsky, J. L. 2002, ApJ, 574, 412

TABLE 1
STELLAR PROPERTIES

HD	Spectral Type	Distance (pc)	A_V (mag)	*ROSAT* (counts/sec)	$\dot{M}_{wind}$ ($\dot{M}_\odot$)	t_{age} (Myr)	Association	Notes
98660	F2V	86	0.08	0.0924	790	∼16	LCC	
103234	F2IV	105	0.06	0.0704	1200	∼16	LCC	
103599	F3IV	91	0.05	0.0395	440	∼16	LCC	
103703	F3V	105	0.09	...	<800	∼16	LCC	
104231	F5V	89	0.07	0.0409	240	∼16	LCC	
104897	F3V	114	0.03	...	<750	∼16	LCC	
105070	G1V	102	0.00	0.219	4600	13	LCC	
106218	F2V	107	0.10	0.0303	640	∼16	LCC	
106444	F5V	101	0.05	0.565	12000	∼16	LCC	
106906	F5V	92	0.02	...	<600	∼16	LCC	
107920	F3V	126	0.03	...	<1200	∼16	LCC	
108568	G1	142	0.00	0.168	6500	14	LCC	
108611	G5V	95	0.00	0.0421	420	10	LCC	
111102	F0III	120	0.00	...	<1100	∼16	LCC	
111104	F0	146	0.11	0.145	4900	∼16	LCC	
112509	F3IV	111	0.00	0.0265	450	∼16	LCC	
113376	G3V	94	0.05	...	<690	?	...	
113556	F2V	102	0.06	...	<750	∼16	LCC	
113766	F3	131	0.01	0.0343	760	∼16	LCC	binary
114082	F3V	83	0.09	...	<470	∼16	LCC	
115600	F2IV	111	0.04	...	<910	∼16	LCC	
117214	F6V	97	0.04	...	<690	∼16	LCC	
117945	F7	92	0.06	...	<620	∼16	LCC	
119022	G2IV	124	0.11	...	<1300	∼16	LCC	
119511	F3V	91	0.01	...	<580	∼16	LCC	
125912	F7V	115	0.12	0.0819	2000	∼17	UCL	
133075	F3IV	137	0.32	...	<1500	∼17	UCL	
136991	F3V	114	0.01	...	<970	∼17	UCL	
137130	F0V	136	0.16	...	<1400	∼17	UCL	
138009	G6V	92	0.00	0.609	12000	7	UCL	
138398	G6III	146	0.00	...	<1900	∼17	UCL	
138994	F2V	149	0.04	...	<1800	∼17	UCL	
139883	F2V	97	0.04	...	<670	∼17	UCL	
142113	F8V	90	0.34	0.119	2000	∼5	US	
143677	G8V	143	0.03	0.409	19000	∼17	UCL	
144225	F3V	119	0.26	0.320	8000	∼17	UCL	
145208	G5V	121	0.08	0.250	11000	∼5	US	
148040	G0V	121	0.00	0.257	8700	∼5	US	
148153	F5V	128	0.03	...	<1300	∼5	US	
152057	F0V	150	0.13	...	<1800	∼5	US	
152404	F5V	145	0.75	...	<1700	∼17	UCL	

NOTE. — LCC = Lower Centaurus Crux, US = Upper Scorpius, UCL = Upper Centaurus Lupus

TABLE 2
Uncolor-Corrected MIPS 24 μm and 70 μm Fluxes

HD	AOR ID	Measured MIPS F_ν(24 μm) (mJy)	Predicted Photosphere F_ν(24 μm) (mJy)	Measured MIPS F_ν(70 μm) (mJy)	Measured 70 μm SNR	Predicted Photosphere F_ν(70 μm) (mJy)	COBE 70 μm Background (MJy sr^{-1})
98660	4778752	10.8	10.9	<33	...	1.2	9.8
103234	4780032	19.3	9.0	<24	...	1.0	18.8
103599	4780544	9.6	9.6	<28	...	1.1	13.2
103703	4780800	26.7	8.0	<33	...	0.9	21.8
104231	4781056	18.4	7.9	<33	...	0.9	17.5
104897	4781312	9.2	8.3	<24	...	0.9	10.9
105070	4781568	9.4	9.2	<23	...	1.0	11.5
106218	4782336	7.7	7.7	<21	...	0.9	16.9
106444	4782848	10.1	9.1	<25	...	1.0	15.9
106906	4783872	108	15.3	290	38	1.7	16.1
107920	4784896	6.0	7.5	<30	...	0.9	21.8
108568	4785152	9.4	9.5	<26	...	1.1	16.9
108611	4785408	9.8	10.7	<41	...	1.2	30.4
111102	4786944	34.1	18.5	<43	...	2.1	24.4
111104	4787200	9.8	10.3	<35	...	1.1	24.4
112509	4787968	7.9	7.7	<39	...	0.9	15.5
113376	4788736	14.3	19.1	<43	...	2.1	31.2
113556	4789504	19.2	9.4	170	14	1.1	24.4
113766	4789760	1470	18.6	350	44	2.1	10.5
114082	4790784	223	11.3	340	15	1.3	40.1
115600	4791552	122	8.6	160	9	1.0	31.1
117214	4792320	207	11.9	300	17	1.3	26.9
117945	4792832	9.5	12.3	<52	...	1.4	29.0
119022	4793344	39.3	40.8	<25	...	4.6	14.9
119511	4793600	10.4	7.4	<29	...	0.8	12.5
125912	4796672	17.0	16.0	<30	...	1.8	12.7
133075	4798720	22.6	15.2	<28	...	1.7	17.8
136991	4800768	7.1	7.7	<43	...	0.9	17.4
137130	4801024	7.5	8.4	<27	...	0.9	20.9
138009	4801536	14.4	12.5	<22	...	1.4	18.1
138398	2802304	27.2	30.2	<44	...	3.4	25.3
138994	4802560	9.6	9.4	<24	...	1.0	17.7
139883	4802816	7.6	7.8	<27	...	0.9	21.2
142113	4804608	9.6	9.6	<27	...	1.1	25.1
143677	4805632	10.0	10.4	<45	...	1.2	29.2
144225	4805888	14.8	15.0	<37	...	1.7	22.6
145208	4806656	10.8	10.9	<28	...	1.2	31.5
148040	4809984	12.9	9.7	<59	...	1.1	47.2
148153	4810240	12.6	10.9	<71	...	1.2	51.1
152057	4812032	8.9	7.9	<28	...	0.9	26.0
152404	4812544	3390	16.8	2840	120	1.2	40.1

TABLE 3
Single Temperature Disk Model Parameters

HD	T_* (K)	L_* ($L_\odot$)	R_* ($R_\odot$)	M_* ($M_\odot$)	T_{gr} (K)	L_{IR}/L_*	D (AU)	M_{dust} (M_{moon})	$\dot{M}_{dust}$ (M_{moon}/yr)	M_{PB} (M_{moon})
103234	7000	4.6	1.4	1.4	...	1.0×10^{-4}	...	...	6×10^{-8}	1
103703	7000	3.9	1.4	...	...	1.9×10^{-4}	...	...	$<8\times10^{-8}$	...
104231	6750	2.6	1.2	...	...	1.4×10^{-4}	...	...	2×10^{-8}	0.3
106906	6750	5.2	1.6	1.4	90	1.4×10^{-3}	20	1×10^{-2}	$<5\times10^{-7}$	...
111102	8000	19.1	2.3	1.8	...	4.3×10^{-5}	...	...	$<2\times10^{-8}$	...
113556	7250	4.8	1.4	1.5	70	7.0×10^{-4}	40	2×10^{-2}	$<3\times10^{-7}$	...
113766	6750	14.1	2.6	1.8	330	2.1×10^{-3}	3	5×10^{-3}	8×10^{-7}	10
114082	6750	3.2	1.3	...	110	3.0×10^{-3}	10	5×10^{-3}	$<8\times10^{-7}$	...
115600	7250	5.2	1.4	1.5	120	1.6×10^{-3}	10	5×10^{-3}	$<8\times10^{-7}$	...
117214	6750	4.6	1.5	1.4	110	2.4×10^{-3}	10	7×10^{-4}	$<9\times10^{-7}$	...
119511	7000	2.5	1.1	...	...	3.8×10^{-5}	...	...	$<1\times10^{-8}$	...
133075	6750	13.5	2.5	1.8	...	3.5×10^{-5}	...	...	$<3\times10^{-8}$	...
148040	6250	4.4	1.8	1.3	...	4.4×10^{-4}	...	...	2×10^{-6}	10

TABLE 4
Optically Thick Disk
Model Parameters

HD	R_{in} (AU)	R_{out} (AU)	i (°)
106906	0.68	∞	68
113556	1.4	∞	60
114082	0.32	∞	63
115600	0.32	∞	72
117214	0.34	∞	63

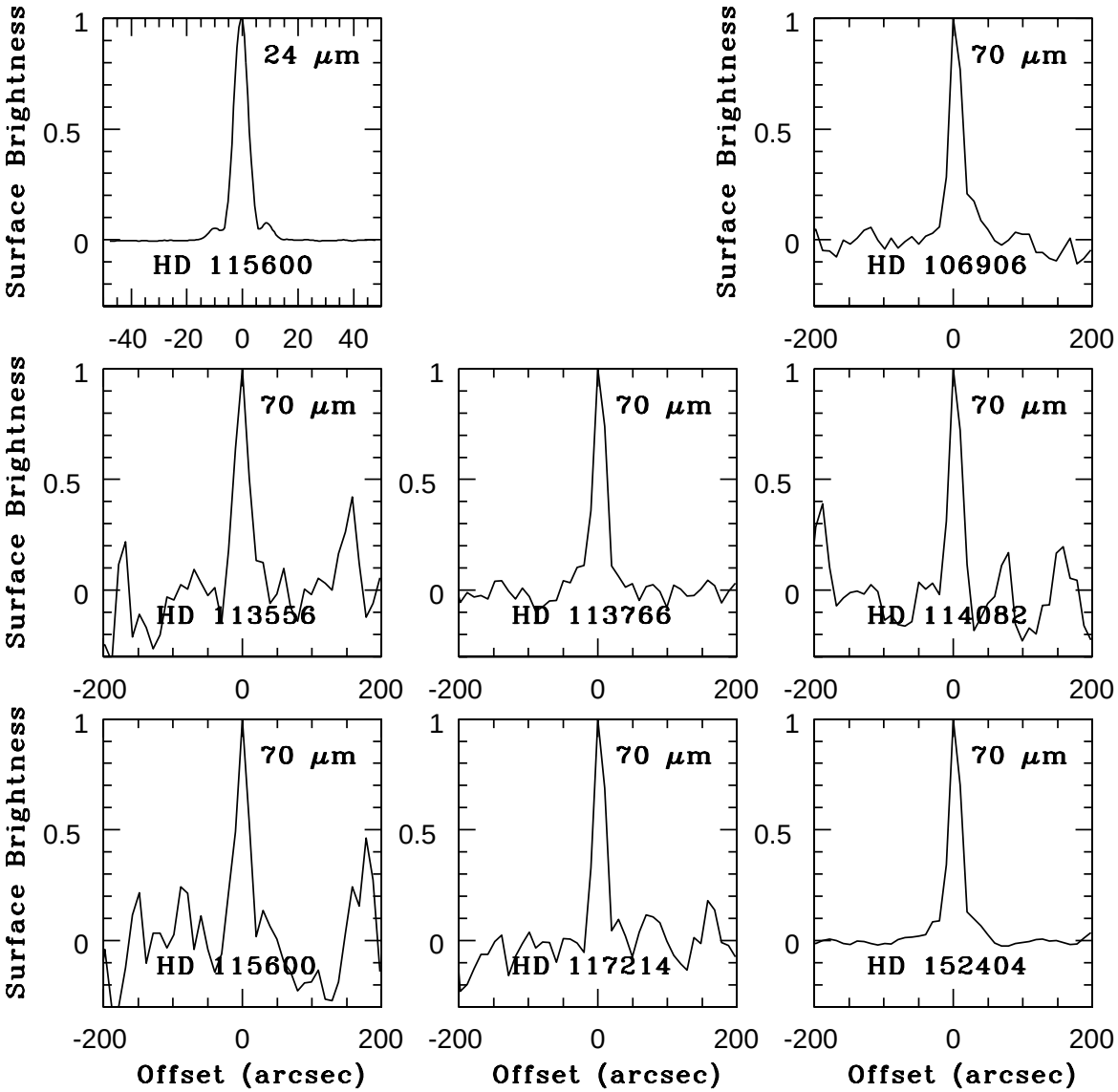

Fig. 1.— Normalized surface brightness line cuts through HD 115600 at 24 μm (representative of all MIPS 24 μm detections in this study) and through all of the 70 μm sources at 70 μm. All sources appear as point source when detected at either wavelength and have positions coincident with *Hipparcos* stellar positions, suggesting that the far-infrared emission is circumstellar and not interstellar.

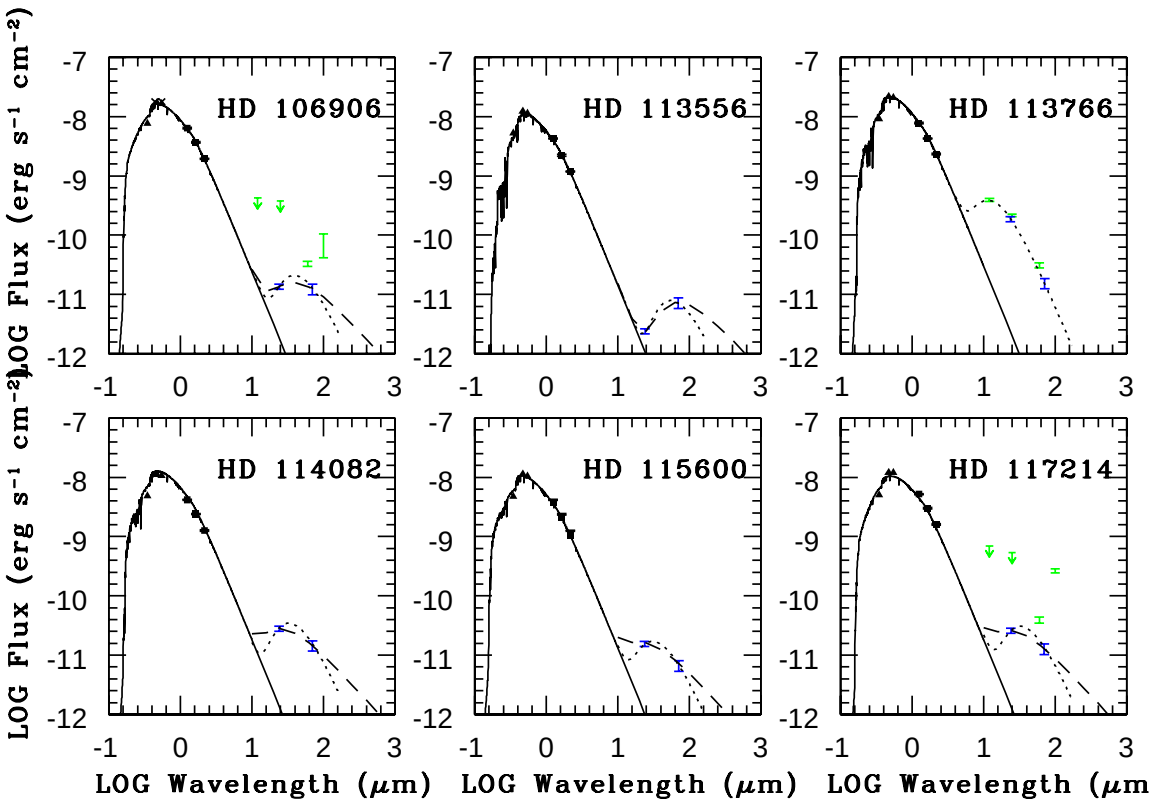

FIG. 2.— Spectral Energy Distributions (SEDs) for objects which possesses 24 μm plus 70 μm excesses: HD 106906, HD 113556, HD 113766, HD 114082, HD 115600, HD 117214. GCPD mean *uvby* fluxes are plotted as triangles, GCPD mean UBV fluxes are plotted as crosses, and 2MASS JHK fluxes (Cutri et al. 2003) are plotted as squares. *IRAS* photometry, where available, is shown with green error bars. Our MIPS 24 μm and 70 μm photometry, as reported here, is shown with dark blue error bars. Overlaid are the best fit 1993 Kurucz model for the stellar atmospheres. The dotted lines are a blackbody fits to the MIPS fluxes at wavelengths longer than 10 μm. The dashed lines are the optically thick models. For HD 106906 and HD 117214, the IRAS 60 μm flux appears brighter than expected from the MIPS 70 μm flux. These lines-of-sight possess high cirrus backgrounds. Structure in the interstellar cirrus observed toward these objects may be better resolved and subtracted in the *Spitzer* data than in the IRAS data.

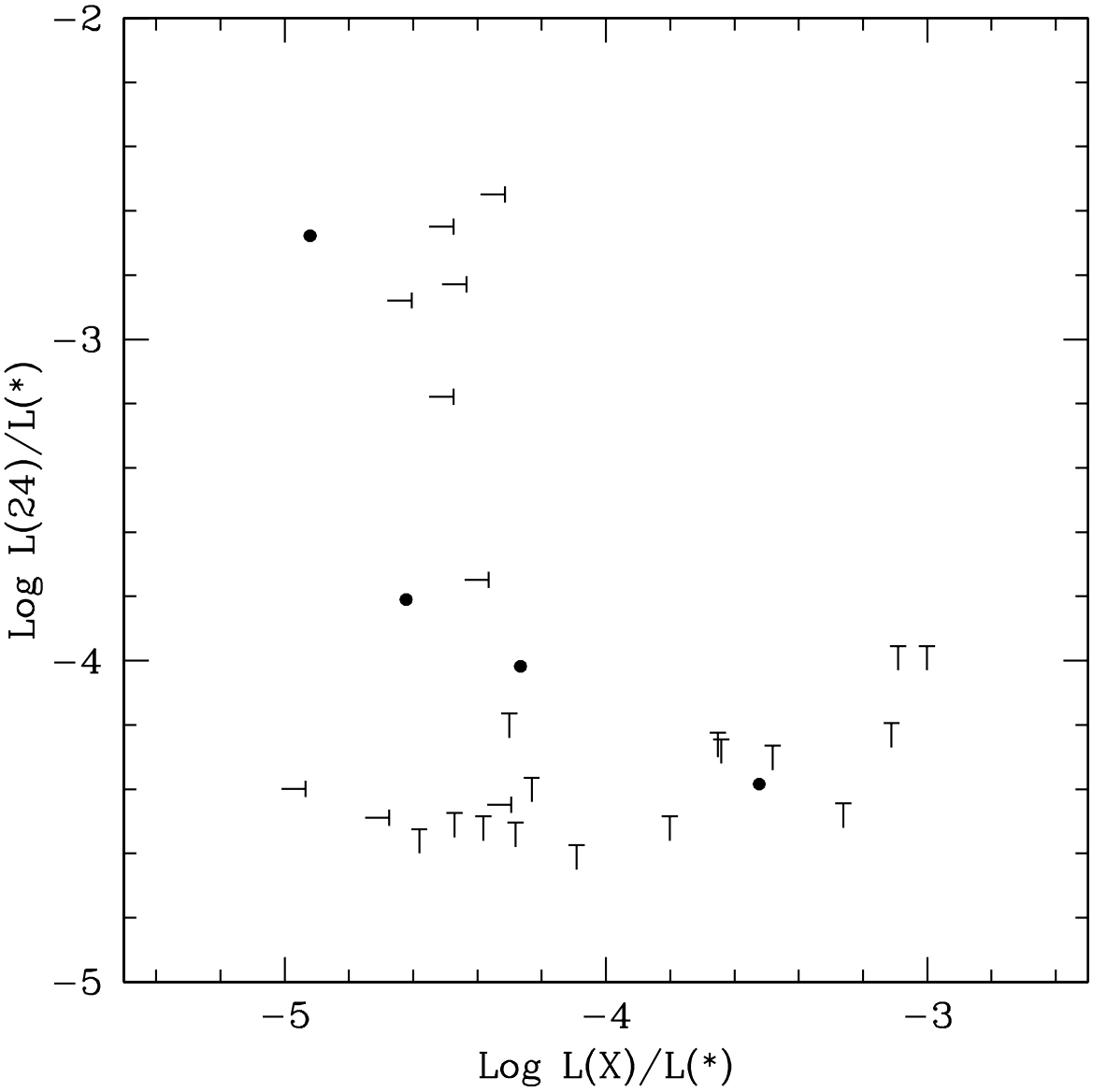

FIG. 3.— Infrared luminosity plotted as a function of stellar x-ray luminosity. Objects plotted as filled circles have both 24 μm excesses and *ROSAT* counterparts. Objects without MIPS 24 μm excesses or without *ROSAT* counterparts are plotted with arrows which show upper limits on the detections.